IEEE Photonics Journal
An IEEE Photonics Society Publication

Open Access

Stable Dual-Wavelength Coherent Source With Tunable Wavelength Spacing Generated By Spectral Slicing a Mode-Locked Laser Using Microring Resonator

Volume 7, Number 6, December 2015

M. R. K. Soltanian
I. S. Amiri
W. Y. Chong
S. E. Alavi
H. Ahmad

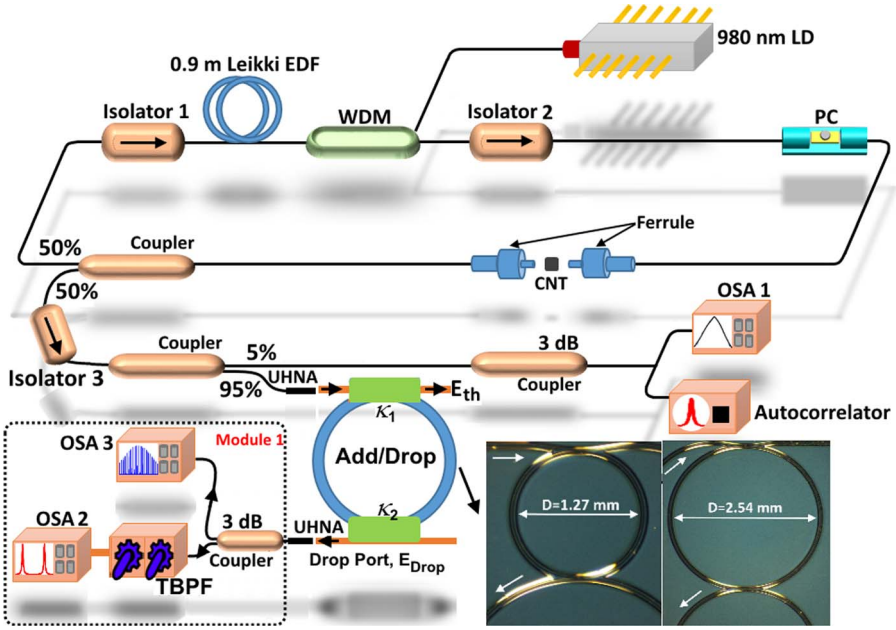

DOI: 10.1109/JPHOT.2015.2504243
1943-0655 © 2015 IEEE

IEEE photonics SOCIETY

IEEE

Stable Dual-Wavelength Coherent Source With Tunable Wavelength Spacing Generated By Spectral Slicing a Mode-Locked Laser Using Microring Resonator

M. R. K. Soltanian,[1] I. S. Amiri,[1] W. Y. Chong,[1] S. E. Alavi,[2] and H. Ahmad[1]

[1]Photonic Research Center, University of Malaya, 50603 Kuala Lumpur, Malaysia
[2]Faculty of Electrical Engineering, Universiti Teknologi Malaysia, 81310 Johor Bahru, Malaysia

DOI: 10.1109/JPHOT.2015.2504243

Manuscript received November 12, 2015; revised November 24, 2015; accepted November 24, 2015. Date of publication November 26, 2015; date of current version December 7, 2015. This work was supported by the University of Malaya/MOHE under Grant UM.C/625/1/HIR/MOHE/SCI/29, Grant LRGS (2015) NGOD/UM/KPT, and Grant RU 007/2015. Corresponding author: H. Ahmad (e-mail: harith@um.edu.my).

Abstract: We demonstrate a stable tunable dual-wavelength erbium-doped fiber laser generated by launching a mode-locked laser into an add–drop microring resonator. Two silicon-based high-index-contrast microring resonators with *Q*-factors of 1.2×10^5 and 0.6×10^5 have been used as add–drop filters independently. As a result, multiwavelength generation was achieved and demonstrated both theoretically and experimentally with free spectral range (FSR) of 0.202 and 0.404 nm corresponding to the microrings' diameter of $D = 2.54$ and $D = 1.27$ mm. A high-resolution tunable bandpass filter and fiber Bragg gratings (FBGs) are then used to extract a tunable and switchable dual-wavelength coherent source from the generated multiwavelength coherent source. Subsequently, the dual-wavelength coherent source with tunable FSRs from 0.404 to 3.232 nm is achieved and presented. The obtained dual-wavelength output has a side-mode suppression ratio of more than 30 dB.

Index Terms: Fiber optics, microring resonators, integrated optics, mode-locked laser pulse, add-drop filter.

1. Introduction

Generation of dual-wavelength fiber lasers (DWFLs) has attracted much research interest recently. They are well known to be useful for applications in the field of optical fiber sensors [1]–[3] which can be used for long haul sensing system and also for optical spectroscopy [4], microwaves photonics systems [5]–[7] and optical wavelength division multiplexing systems (WDM) [8], [9]. Other useful applications are optical component testing, optical instrumentation and characterization of photonics components such as chromatic dispersion measurement [10].

Zhou *et al.* have proposed a stable dual-wavelength laser based on cascaded fiber Bragg gratings [11], whereby the laser wavelengths are determined by the fiber Bragg gratings (FBGs) and thus the wavelength spacing is fixed by the centre wavelengths of the FBGs pair. On the other hand, a dual-wavelength laser proposed in [12] that employs a Sagnac loop mirror made by a 145.5 cm polarization maintaining fiber which is switchable, tunable, and stable room

temperature operation. Another configuration of tunable dual-wavelength is demonstrated in [13], wherein a high birefringence FBG stabilizes a dual-wavelength laser produced when the polarization state of each wavelength is altered using a polarization controller. A large number of researchers have investigated the distinctive properties of photonic crystal fibers, such as wide range single mode operation, dispersion flexibility, large mode area, and its application in multi-wavelength generation [14]–[18]. In most cases, these properties were proven to be wavelength dependent and equivalent to the behavior of wavelength-selective filters [19], [20]. Nevertheless, achieving dual wavelength generation in the 1, 1.5, and 2.0 μm wavelength regions with ytterbium doped fibers (YDFs), erbium doped fibers (EDFs), and thulium doped fiber (TDFLs) respectively, remains challenging due to strong mode competition caused by homogeneous gain broadening in these gain media. Various approaches for overcoming this setback have been reported for erbium-doped fiber lasers, which include four wave mixing [21], polarization hole burning [22] and cascaded stimulated Brillouin scattering [23]. Recently, DWFLs have also been demonstrated through the use of dual-wavelength vertical external cavity surface emitting laser (VECSEL) based on intracavity difference frequency generation (DFG) mixing in a nonlinear crystal for generating THz radiations [24]. However, this approach may have limited applications, as the proposed system requires the use of a very high power pump laser operating at 808 nm with an output of approximately 50 W in order to obtain the desired dual-wavelength output at 1030 nm from the VECSEL, therefore making this approach highly suited for laboratory environments. Hence, the generation of stable and tunable dual-wavelength laser source at moderate pump power is very much desired.

The narrowband filtering property of microring resonators has been investigated and demonstrated. Silicon-based high index contrast microring resonators have been used as bandpass filters, demultiplexers in DWDM systems [25], [26] and add-drop filters [27]–[32]. Application as a single wavelength microring mirror with a reflection full width at half maximum (FWHM) of 0.4 nm was also reported [33]. The use of microring resonator outside the ring laser cavity infer a cavity polarization independency to generate stable DWFLs which bring advantages of flexibility and wavelength-dependent characteristics, thus making the material an almost ideal choice as a wavelength selective filter.

In this paper, generation of multi-wavelength coherent source operating at 1.5 μm by utilizing microring resonator is investigated and demonstrated both theoretically and experimentally. The generated multi-wavelength has maximum power in its central wavelength at 1560 nm. Subsequently, stable and tunable dual-wavelength (DW) coherent source outputs are obtained from a mode-locked laser spectrum sliced by an add-drop microring resonator with the aid of a tunable bandpass filter (TBPF) and a FBG. The evolution of the theory of mode-locking has been reviewed and some of the salient experiments have been discussed in the context of the theory in [34]. Two silicon oxynitride (SiOxNy) microring resonators with different diameters are used as narrowband filter for the generation of stable tunable dual-wavelength lasers with variable free spectral range (FSR) accordingly. Extraction of DW coherent source signals is demonstrated with side mode suppression of more than 30 dB. The microring resonator can be readily integrated into a photonics integrated chip (PIC) for multifunctional applications as the achieved FSR is in linear relation with the ring resonators' diameter.

2. Experimental Setup

Fig. 1 shows the experimental setup employed for stable tunable dual-wavelength laser generation, in which the fiber laser layout consists of a mode-locked ring laser connected to a single add-drop microring resonator filter. The ring laser utilized a 0.9 m long high concentration erbium-doped fiber (EDF) (Leikki Er80-8/125) as gain medium. The numerical aperture (NA) of the EDF is 0.21, with an absorption coefficient of 84 dB/m at 980 nm and mode field diameter of 5.7 μm at 1550 nm. The EDF was backward-pumped by a Lumics 980 nm laser diode (LD) through a wavelength division multiplexer (WDM). One end of the EDF was connected to the common or signal port of the WDM, while the other end was connected to isolator 1 to ensure

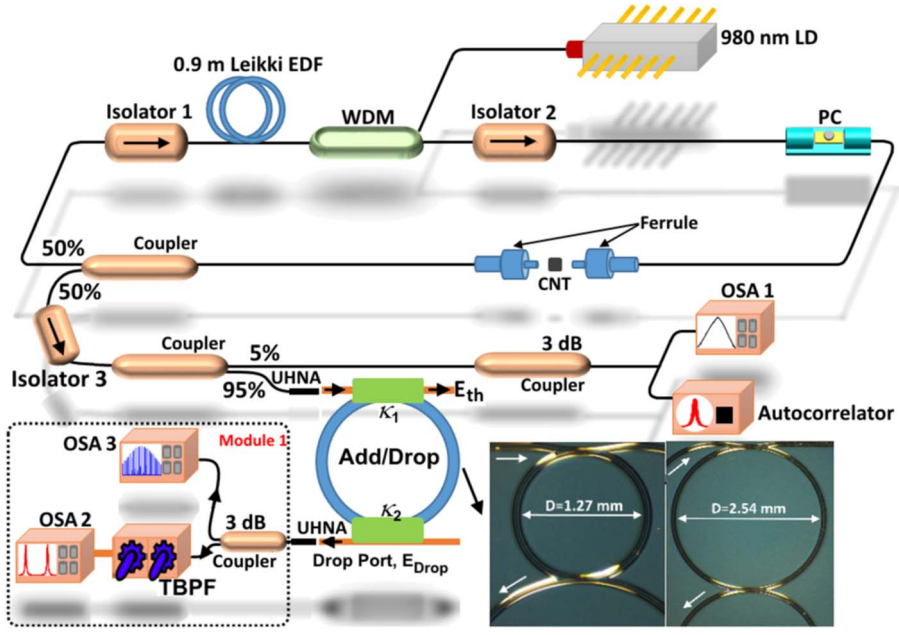

Fig. 1. Experimental setup to generate stable tunable dual-wavelength.

unidirectional light propagation in the laser cavity. Isolator 2 was connected between the WDM and the polarization controller (PC) to prevent unwanted back reflections from the PC towards the gain medium. The PC was subsequently connected to a carbon nanotube (CNT) embedded between two ferrules which acts as the saturable absorber. The output of the embedded CNT was guided towards a 50:50 coupler, which extracts a portion of the signal for analysis. One of the 50% port was connected to isolator 1, which was then connected to the gain medium. This loop completes the laser cavity.

In order to generate the stable tunable dual-wavelength laser, the 50% output port was divided into two portions using a 95:5 coupler through isolator 3, and the 95% port was spliced to a 10 cm Ultra-high numerical aperture (UHNA) fiber with NA of 0.41 using a fusion splicer (Fujikura 45 PM). The UHNA fiber was then aligned with the microring resonators using the three-axis linear alignment stage for the generation of evenly spaced multi-wavelength comb spectrum. The 5% port of the coupler was utilized for monitoring purposes. In order to monitor the extracted output prior to the microring resonator, the generated mode-locked signal from the 5% port was divided into two portions with equal power using a 3 dB coupler; one portion was directed to an optical spectrum analyzer (OSA1) (YOKOGAWA AQ6370B) for spectral analysis, while the other portion to an autocorrelator to measure the pulsewidth. Output from the microring resonator was coupled to a 3 dB coupler through a 10 cm long UHNA fiber. One of the 50% output of the 3 dB coupler is then connected to a high resolution OSA2 (APEX AP2051A) via tunable bandpass filter (Yenista xtm-50) with a wavelength resolution of 5 pm and FWHM of 1 pm to select the desired wavelength pair from the generated multi-wavelength output comb. The OSA3 (YOKOGAWA AQ6370B) was used to monitor the generated multi-wavelength output comb.

Silicon oxynitride (SiOxNy) microring resonators were used as the narrow bandpass filter. The SiON film deposited using plasma enhanced chemical vapor deposition (PECVD) has refractive index of 1.513. The film was deposited on a silicon substrate with a 15 μm thick thermal oxide layer as an under cladding buffer. Waveguides are defined through reactive ion etching (RIE) followed by deposition of a borophosphosilicate glass (BPSG) layer as the over cladding. The refractive index contrast is 4.5%. The input and output ports of the microring resonators are shown in the inset of Fig. 1. The SiON microring resonators have a small footprint of 3×5 mm^2. The finesse (F), which is given by the ratio FSR/FWHM, was approximately 15.53.

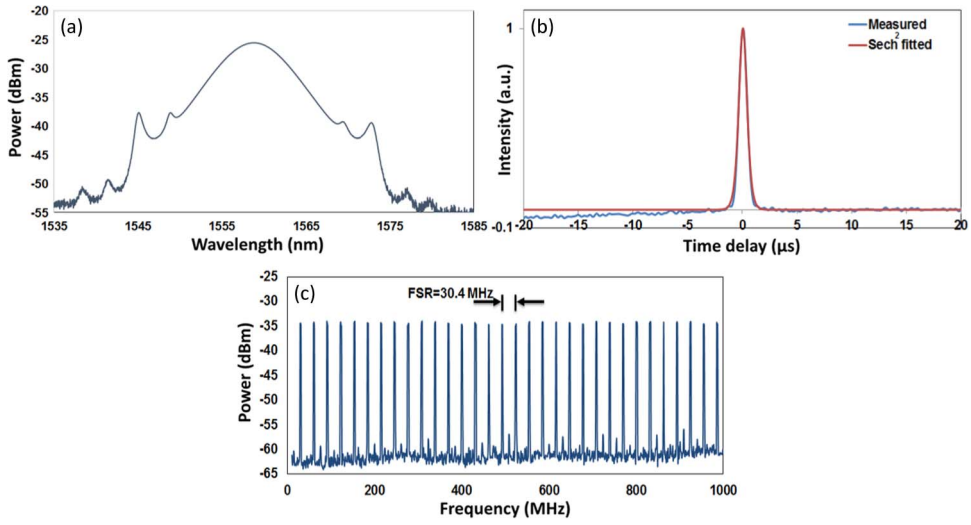

Fig. 2. (a) Mode-locked laser spectrum taken from OSA 1, (b) autocorrelator trace of the generated mode-lock, and (c) RF spectrum of the generated mode-locked laser with FSR = 30.4 MHz.

Two microrings having diameters of 2.54 and 1.27 mm were used, and their Q factors are 1.2×10^5 and 0.6×10^5 respectively. Using the time-bandwidth product for the case of mode-locked laser or solitons which is 0.32, the minimum pulse duration of laser pulses after microring resonator filtering are approximately 200 and 100 ps for the microring resonators having diameters of 2.54 and 1.27 mm, respectively.

3. Results and Discussion

Mode-locked fiber laser was generated by incorporating CNT polymer composite as a saturable absorber (SA) in the ring laser cavity. A small piece of CNT composite with an area of 1 mm^2 is placed carefully on the top of a fiber ferrule by using a very thin layer of index matching gel (IMG) on its surface. The ferrule with the CNT layer is then connected to an FC/PC adaptor, and a second fiber ferrule with a clean surface is then connected to this adaptor, thereby sandwiching the CNT layer in between the two ferrules and thus creating the required SA. Mode-locked laser is achieved with a launched pump power of 50 mW, with the laser optical spectrum measured using the OSA 1. The laser spectrum is shown in Fig. 2(a).

The corresponding pulsewidth of the mode-locked laser while an Alnair HAC-200 autocorrelator (including an embedded electrical amplifier) was used to measure the pulse profile is shown in Fig. 2(b). The estimated pulse durations at the full-width at half maximum (FWHM) point is 570 fs. The autocorrelation trace and spectrum are well fitted by a $sech^2$ pulse profile, indicating that mode-locked laser is generated. Fig. 2(c) shows the RF spectrum of the generated mode-locked laser taken by Anritsu MS2667C RF spectrum analyzer. To achieve this result, the RF spectrum analyzer replaced by the OSA1 in the main configuration setup shown in Fig. 1. The free spectral range of the optical ring resonator (cavity) is the frequency spacing of its axial (Gaussian-shaped) resonator modes. It is therefore also called axial mode spacing. For a standing-wave ring resonator filled with CNT as dispersive medium, the FSR or Δv is determined by the group index (n_g), rather than by the ordinary refractive index:

$$\Delta v = \frac{c}{n_g L} \tag{1}$$

where c is the speed of light in vacuum, and L is the total length of optical path around the ring. The FSR of 30.4 MHz shown in Fig. 2(c) is a result of beating of the adjacent modes generated by mode-locked laser. Introducing a delay line increases the L, the total length of optical path

around the ring cavity, and, consequently, decreases the FSR. Moreover, introducing an optical delay line in the mode-locked laser cavity enables fine-tuning of the cavity length, such that the modal spacing could be accurately defined [35]. The generated mode-locked laser is then launched into two different microring resonators independently using fiber butt-coupling technique. To minimize coupling loss between SMF and the microring resonator, short length of UHNA fibers were spliced to the two end of SMF, as shown schematically in Fig. 1, and the splice loss of 0.5 dB for each side was achieved. Using three 3-axis linear alignment stages to couple the mode-locked laser into and out of the microring resonator, the insertion loss of the microring resonator was measured to be 16 dB. The problem of coupling an optical fiber to a waveguide (or a waveguide to a fiber) is critically important for overall performance of integrated/fiber-optic systems. The most straight forward way of coupling a fiber and a waveguide is a butt coupling technique in which the two are aligned end to end and butted into contact. The key factors affecting butt coupling between a fiber and a waveguide are area mismatch between the waveguide cross-sectional area and that of the fiber core, misalignment of the waveguide and fiber axes, and numerical aperture loss (caused by that part of the waveguide light output profile that lies outside of the fiber's acceptance core or *vice versa*). In the case of butt coupling of the semiconductor waveguide and a glass laser, reflection at the glass-air-semiconductor interface are also important. The insertion loss problem becomes more important as the refractive-index contrast of the integrated optical waveguides Δ, which is given by the core refractive index n_{co} and the cladding refractive index n_{cl}, is increased [36]:

$$\Delta = \frac{n_{co}^2 - n_{cl}^2}{2n_{co}^2} \approx \frac{n_{co} - n_{cl}}{n_{co}}. \tag{2}$$

To achieve a good match to optical fibers, silica waveguides are usually designed to have Δ in the range 0.3–0.7%. In considering coupling of light from the fiber into the waveguide, the problems of area mismatch and numerical aperture loss are limiting factors because the core diameter of a single mode fiber is approximately 4–10 μm and the rectangular waveguide dimensions are 1–5 μm. Exact calculation of the coupling efficiency from fiber to waveguide cannot be done until a particular waveguide and optical fiber have been selected and their characteristics known; however, a typical experimentally observed coupling efficiency for this situation would be about 10% [37]. Robertson *et al.* [38] have performed a theoretical analysis of butt coupling between a semiconductor rib waveguide and a single mode fiber, and have designed an optimized waveguide structure with a large (single) mode size for which they calculate a coupling efficiency of 86%. However, no experimental data is available. To obtain efficient coupling between optical fibers and waveguides very accurate alignment of the fiber and waveguide is required. Fiber positioning systems provide repeatable accuracy of 0.1 μm.

The most basic type of optical resonator is the Fabry-Perot cavity resonator, which is the archetype of optical devices. The Fabry-Perot cavity is comprised of two parallel reflective planes separated by a distance *L*. An important parameter used to measure the resolution of a resonator is the finesse. A Fabry-Perot could have a relatively high finesse intensity transmission but has a low finesse reflection transmission. Subsequently, difficult integration on a chip and low finesse intensity reflection are the two main disadvantages of Fabry-Perot. To improve the integration of a Fabry-Perot resonator on a semiconductor chip is to use a ring resonator, which does not require the use of any cleaved facet. The critical distance in a ring resonator is defined by the circumference of circular waveguide rather than the separation between two reflective planes as in a traditional Fabry-Perot resonator. Although ring resonators establish resonance in a similar manner to the Fabry-Perot resonator, the advantages of a ring resonator over the Fabry-Perot is its ease of integration and higher finesse intensity transmission, but its disadvantage is that it does not reflect back any field.

The inherent property of microring resonator as a filter is due to interference of light with itself and, consequently, excitation of constructive and destructive modes. Evenly spaced modes with equal FSR are selected and passed from the microring resonator. For the add-drop system, the

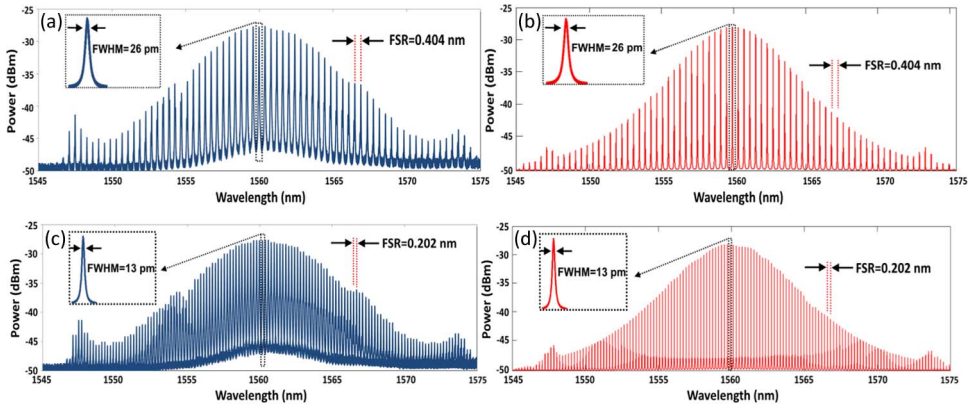

Fig. 3. (a) Output spectrum of microring resonator with D = 1.27 mm taken from OSA 3, (b) MATLAB modeling results for microring resonator with D = 1.27 mm, (c) output spectrum of microring resonator with D = 2.54 mm taken from OSA 3, and (d) MATLAB modeling results for microring resonator with D = 2.54 mm.

interior electric fields E_a and E_b are expressed as [39]

$$E_a = \frac{E_{in} \times j\sqrt{\kappa_1}}{1 - \sqrt{1-\kappa_1}\sqrt{1-\kappa_2}e^{\frac{-\alpha}{2}L_{ad} - jk_nL_{ad}}} \tag{3}$$

$$E_b = \frac{E_{in} \times j\sqrt{\kappa_1}}{1 - \sqrt{1-\kappa_1}\sqrt{1-\kappa_2}e^{\frac{-\alpha}{2}L_{ad} - jk_nL_{ad}}} \cdot \sqrt{1-\kappa_2}e^{\frac{-\alpha}{2}\frac{L_{ad}}{2} - jk_n\frac{L_{ad}}{2}} \tag{4}$$

where $\kappa_1 = 0.1$ and $\kappa_2 = 0.1$ are the coupling coefficients, and $L_{ad} = 2\pi R_{ad}$, and R_{ad} is the radius of the add-drop microring resonator. $k_n = 2\pi/\lambda$ is the wave propagation number in a vacuum and $\alpha = 0.5$ dBmm^{-1} is the linear absorption coefficient. The MATLAB modeling uses iterative method to obtain the presented results. The throughput and drop ports electrical fields of the add-drop microring resonator can be expressed as

$$\begin{aligned}\frac{E_{th}}{E_{in}} &= \frac{-\kappa_1\sqrt{1-\kappa_2}e^{\frac{-\alpha}{2}L_{ad} - jk_nL_{ad}} + \sqrt{1-\kappa_1} - (1-\kappa_2)\sqrt{1-\kappa_2}e^{\frac{-\alpha}{2}L_{ad} - jk_nL_{ad}}}{1 - \sqrt{1-\kappa_1}\sqrt{1-\kappa_2}e^{\frac{-\alpha}{2}L_{ad} - jk_nL_{ad}}} \\ &= \frac{-\sqrt{1-\kappa_2}e^{\frac{-\alpha}{2}L_{ad} - jk_nL_{ad}} + \sqrt{1-\kappa_1}}{1 - \sqrt{1-\kappa_1}\sqrt{1-\kappa_2}e^{\frac{-\alpha}{2}L_{ad} - jk_nL_{ad}}}\end{aligned} \tag{5}$$

$$\frac{E_{drop}}{E_{in}} = \frac{-\sqrt{\kappa_1.\kappa_2}e^{\frac{-\alpha}{2}\frac{L_{ad}}{2} - jk_n\frac{L_{ad}}{2}}}{1 - \sqrt{1-\kappa_1}\sqrt{1-\kappa_2}e^{\frac{-\alpha}{2}L_{ad} - jk_nL_{ad}}}. \tag{6}$$

The normalized optical outputs of the microring resonator can be expressed by (5) and (6)

$$\frac{|E_{th}|^2}{|E_{in}|^2} = \frac{(1-\kappa_1) - 2\sqrt{1-\kappa_1}\cdot\sqrt{1-\kappa_2}e^{-\frac{\alpha}{2}L_{ad}}\cos(k_nL_{ad}) + (1-\kappa_2)e^{-\alpha L_{ad}}}{1 + (1-\kappa_1)(1-\kappa_2)e^{-\alpha L_{ad}} - 2\sqrt{1-\kappa_1}\cdot\sqrt{1-\kappa_2}e^{-\frac{\alpha}{2}L_{ad}}\cos(k_nL_{ad})} \tag{7}$$

$$\frac{|E_{drop}|^2}{|E_{in}|^2} = \frac{\kappa_1\kappa_2 e^{-\frac{\alpha}{2}L_{ad}}}{1 + (1-\kappa_1)(1-\kappa_2)e^{-\alpha L_{ad}} - 2\sqrt{1-\kappa_1}\cdot\sqrt{1-\kappa_2}e^{-\frac{\alpha}{2}L_{ad}}\cos(k_nL_{ad})} \tag{8}$$

where $|E_{th}|^2$ and $|E_{drop}|^2$ are the optical output powers of the throughput and drop ports, respectively.

Fig. 3(a) shows the multi-wavelength output spectrum measured using OSA 3 when the microring resonator with the diameter of 1.27 mm was used. The MATLAB modeling for the mentioned configuration is illustrated in Fig. 3(b). The MATLAB modeling uses iterative method to obtain the presented results.

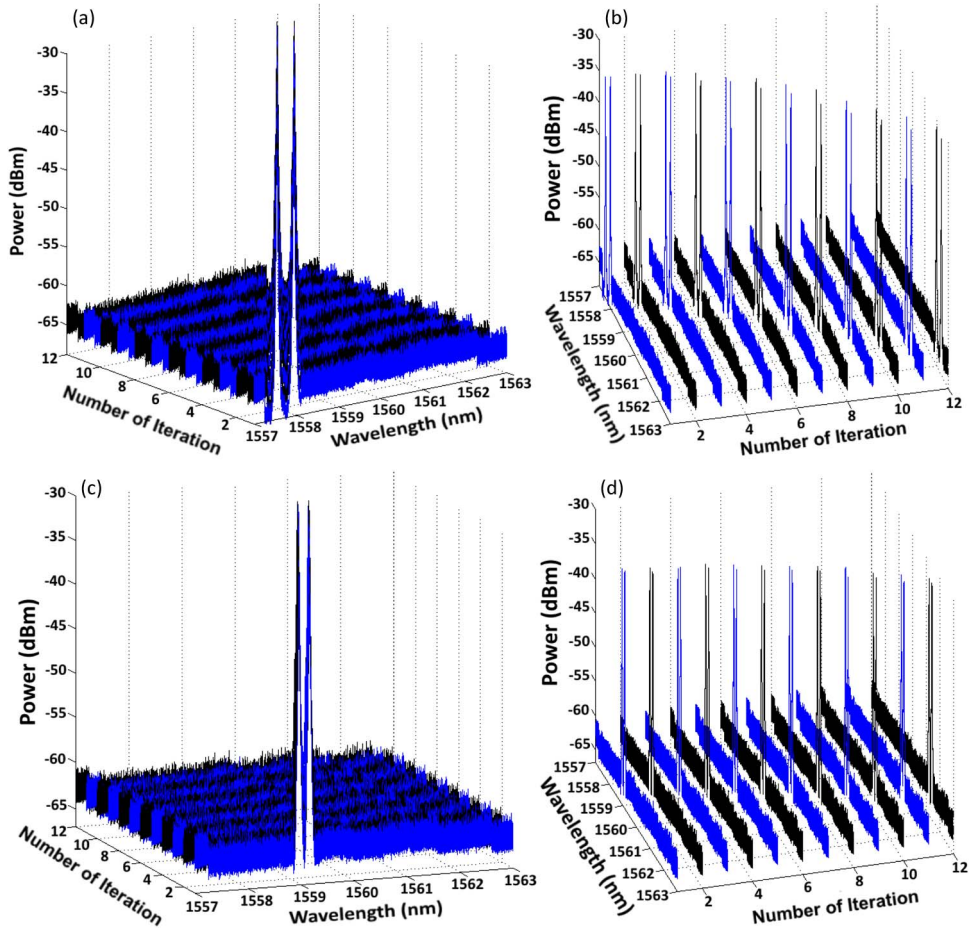

Fig. 4. (a) and (b) Tunability of generated dual-wavelength when microring resonator with D = 1.27 mm was used. (c) and (d) Tunability of generated dual-wavelength when microring resonator with D = 2.54 mm was used.

Achieving same FSR and FWHM of 0.404 nm and 26 pm, respectively, from the results obtained from OSA3 and MATLAB simulation for the setup utilizing microring resonator with D = 1.27 mm is a fidelity confirmation of both experimental and modeling results. The same experiment has been carried out utilizing microring resonator with D = 2.54 mm. The experimental and modeling output spectrums are shown in Fig. 3(c) and (d), respectively. FSR and FWHM of 0.202 nm and 13 pm were achieved respectively from the results obtained from OSA3 and MATLAB simulation. By fine tuning the bandwidth of high resolution TBPF, desirable dual-wavelength pair from the generated multi-wavelength output were filtered out, as shown in Fig. 4.

Fig. 4(a) and (b) shows the tunability of generated DW coherent source vary in the range of 1557 to 1563 nm by varying the TBPF in two different views while the microring resonator with D = 1.27 mm was used. Similarly, Fig. 4(c) and (d) shows the same results when the microring resonator with D = 2.54 mm was utilized. The number of iteration corresponds to displacement of the TBPF in each steps. The stability of generated DW coherent sources are shown in Fig. 5. The stability of generated DW coherent source utilizing the microring resonator with D = 1.27 mm over 300 minutes with every scan at time interval of 30 minutes is illustrated in Fig. 5(a) and (b) in different view. The DW coherent source center wavelengths were 1559.568 and 1559.972 nm.

The stability of generated DW coherent source utilizing microring resonator with D = 2.54 mm shown in Fig. 5(c) and (d) during 300 minutes with interval scan for every 30 minutes. The DW

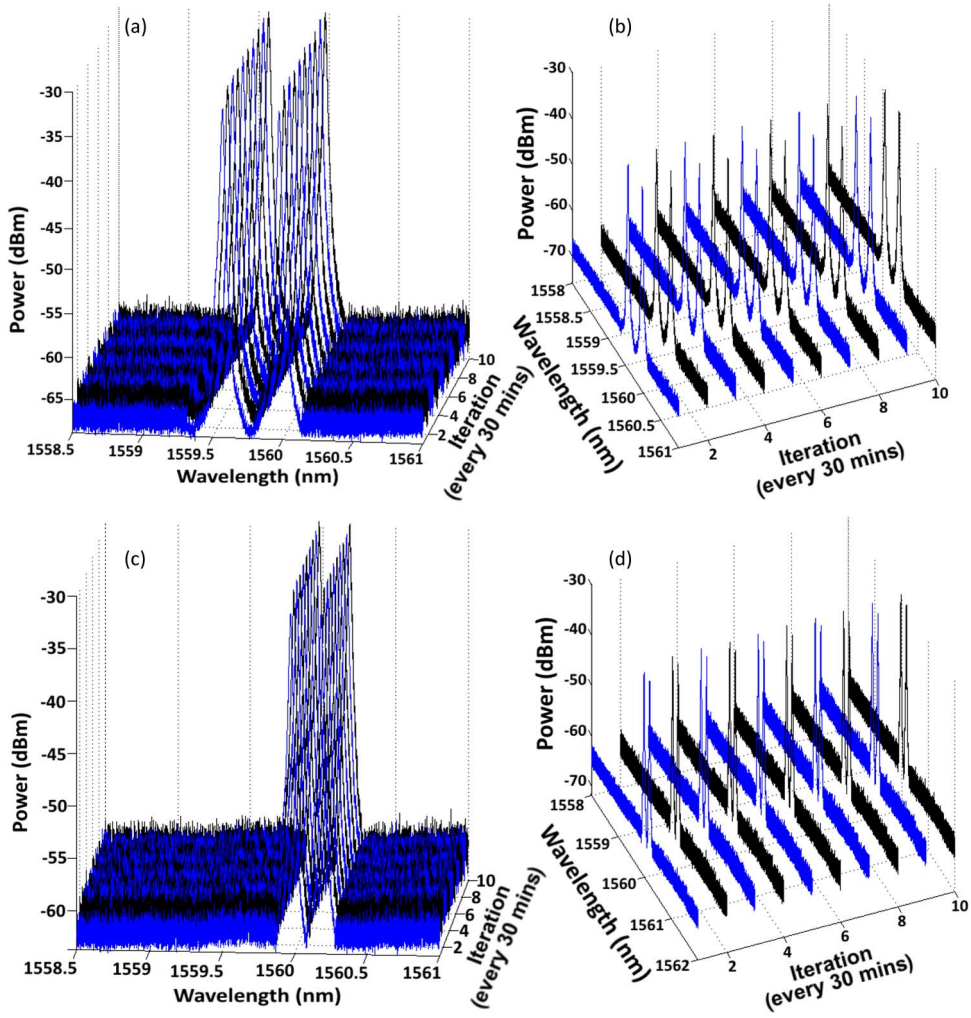

Fig. 5. (a) and (b) Stability of generated DW coherent source at wavelengths of 1559.568 and 1559.972 nm over 300 min. (c) and (d) Stability of generated DW coherent source at wavelengths of 1559.972 and 1560.174 nm over 300 min.

coherent source centre wavelengths were 1559.972 and 1560.174 nm. Fig. 6(a) shows the power fluctuation of the generated DW coherent source utilizing the microring resonator with D = 1.27 mm over 300 minutes. The power is very stable during the period of experiment at room temperature. Fig. 6(b) shows the same procedure for the setup utilizing microring resonator with D = 2.54 mm.

The DW coherent source with different independent FSR were achieved by replacing the module 2 configuration setup shown in Fig. 7 by the module 1 shown in Fig. 1 in the main configuration setup. By utilizing module 2 instead of module 1, the generated multi-wavelength is divided in two arms by a 3 dB coupler as shown in Fig. 7. Consequently the average power of the generated multi-wavelength is decreased by 3 dB in each arm. The upper arm contains the high resolution TBPF set the FWHM so that can pass only one wavelength. The lower arm contains a 3 port circulator and a FBG with the center wavelength of 1561.687 nm, FWHM of 0.232 nm and insertion loss of 0.27 to filter out the generated wavelength at 1561.558 nm.

By fine tuning the TBPF when the microring resonator with D = 1.27 mm used, the stable and tunable DW coherent source achieved as shown in Fig. 8. The achieved tunable FSR's are integer coefficient of the minimum achieved FSR, which is 0.404 nm.

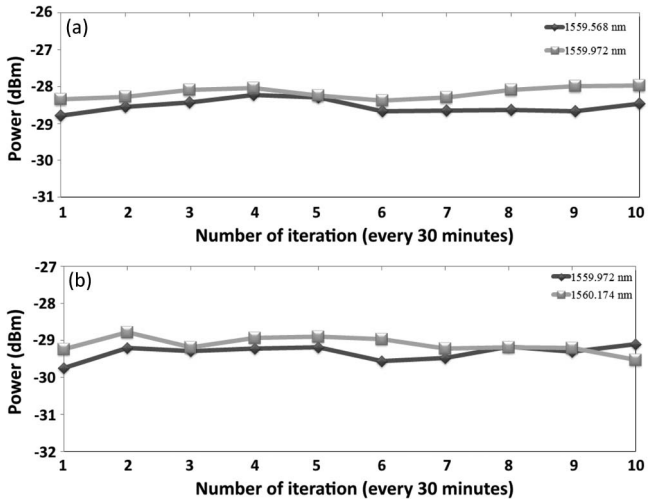

Fig. 6. Power stability of generated DW coherent source over 300 min for the wavelengths of (a) 1559.568 and 1559.972 nm and (b) 1559.972 and 1560.174 nm.

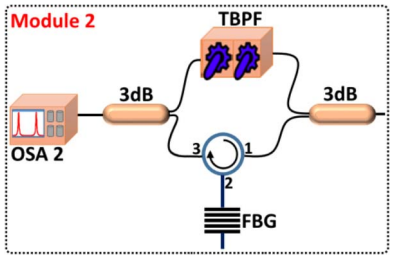

Fig. 7. Configuration setup as module 2 to place in the main setup instead of module 1 to generate tunable DW coherent source with different FSR.

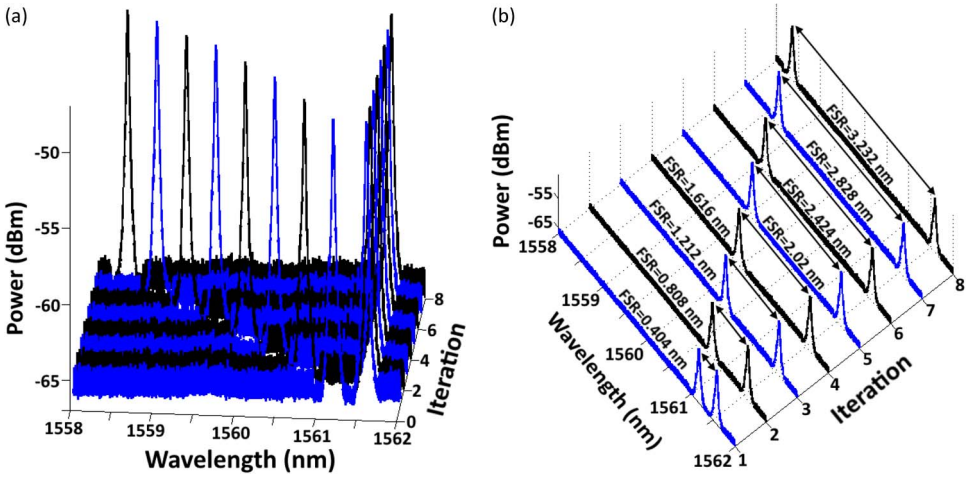

Fig. 8. (a) and (b) Generation of DW coherent source with different independent FSRs in two different views.

Fig. 8 shows the tunability of achieved FSR from 0.404 to 3.232 nm in two different views. Since the stable DW coherent sources are playing a very important role in applications such as optical spectroscopy, microwaves photonics systems, optical wavelength division multiplexing systems (WDM), CW THz radiation signals, optical component testing and chromatic dispersion measurement, the linear relation between the microrings' resonator diameter and FSR of the generated DW coherent source infer to pre-design accurate optics, and photonics on chip devices.

4. Conclusion

A tunable stable DW coherent source have been studied and demonstrated experimentally by launching mode-locked laser pulses with a FWHM pulse duration of 570 fs into a microring resonator. Moreover, generation of multiwavelength coherent source operating at 1.5 μm by utilizing microring resonator is investigated and demonstrated both theoretically and experimentally. The experimental results were in agreement with the MATLAB modeling results. The SiO_xN_y microring resonators have a small footprint of 3×5 mm^2. The finesse (F), given by the ratio FSR/FWHM, was approximately 15.53, where the Q factors of the two microring resonators having diameters of 2.54 and 1.27 mm are 1.2×10^5 and 0.6×10^5 respectively. Regarding the time-bandwidth product which is 0.32 for the case of mode-locked laser or solitons, the minimum pulse duration calculated are 200 and 100 ps for the microring resonators having diameters of 2.54 and 1.27 mm, respectively. The FSR of 0.202 and 0.404 nm and FWHM of 13 and 26 pm were achieved by the setup utilizing add-drop microring resonator with $D = 2.54$ and $D = 1.27$ mm, respectively. Obtaining higher FSR as integer coefficient of the minimum achieved FSR results from utilizing FBG and TBPF together. The dual wavelength fiber laser showed stable operation at room temperature with both wavelength and power. It has more than 30 dB optical signal-to-noise-ratio. The authors anticipate that the success of the design described here will spur further research efforts and application in this area.

References

[1] P.-C. Peng, H.-Y. Tseng, and S. Chi, "Long-distance FBG sensor system using a linear-cavity fiber Raman laser scheme," *IEEE Photon. Technol. Lett.*, vol. 16, no. 2, pp. 575–577, Feb. 2004.

[2] G. Bolognini, M. A. Soto, and F. D. Pasquale, "Fiber-optic distributed sensor based on hybrid Raman and Brillouin scattering employing multiwavelength Fabry-Pérot lasers," *IEEE Photon. Technol. Lett.*, vol. 21, no. 20, pp. 1523–1525, Oct. 2009.

[3] L. Talaverano, S. Abad, S. Jarabo, and M. Lopez-Amo, "Multiwavelength fiber laser sources with Bragg-grating sensor multiplexing capability," *J. Lightw. Technol.*, vol. 19, no. 4, pp. 553–558, Apr. 2001.

[4] J. Marshall, G. Stewart, and G. Whitenett, "Design of a tunable L-band multi-wavelength laser system for application to gas spectroscopy," *Meas. Sci. Technol.*, vol. 17, no. 5, pp. 1023–1031, Apr. 2006.

[5] J. Capmany *et al.*, "Multiwavelength single sideband modulation for WDM radio-over-fiber systems using a fiber grating array tandem device," *IEEE Photon. Technol. Lett.*, vol. 17, no. 2, pp. 471–473, Feb. 2005.

[6] Y. Yao, X. Chen, Y. Dai, and S. Xie, "Dual-wavelength erbium-doped fiber laser with a simple linear cavity and its application in microwave generation," *IEEE Photon. Technol. Lett.*, vol. 18, no. 1, pp. 187–189, Jan. 2006.

[7] J. Sun, Y. Dai, X. Chen, Y. Zhang, and S. Xie, "Stable dual-wavelength DFB fiber laser with separate resonant cavities and its application in tunable microwave generation," *IEEE Photon. Technol. Lett.*, vol. 18, no. 24, pp. 2587–2589, Dec. 2006.

[8] J. Pan, "Multiwavelength photonic communications," in *Proc. Nat. Telesyst. Conf. Commercial Appl. Dual-Use Technol.*, 1993, pp. 15–20.

[9] X. Feng *et al.*, "WDM-PON using Fabry–Pérot laser diodes injection locked by multiwavelength erbium-doped fiber laser," in *Proc. 16th Opto-Electron. Commun. Conf.*, 2011, pp. 523–524.

[10] J.-N. Maran, R. Slavík, S. LaRochelle, and M. Karásek, "Chromatic dispersion measurement using a multiwavelength frequency-shifted feedback fiber laser," *IEEE Trans. Instrum. Meas.*, vol. 53, no. 1, pp. 67–71, Feb. 2004.

[11] P. Zhou, X. L. Wang, Y. X. Ma, K. Han, and Z. J. Liu, "Stable all-fiber dual-wavelength thulium-doped fiber laser and its coherent beam combination," *Laser Phys.*, vol. 21, no. 1, pp. 184–187, Jan. 2011.

[12] S. E. Alavi, I. S. Amiri, H. Ahmad, A. S. M. Supa'at, and N. Fisal, "Generation and transmission of 3×3 W-band MIMO-OFDM-RoF signals using micro-ring resonators," *Appl. Opt.*, vol. 53, no. 34, pp. 8049–8054, Dec. 2014.

[13] S. Liu *et al.*, "Tunable dual-wavelength thulium-doped fiber laser by employing a HB-FBG," *IEEE Photon. Technol. Lett.*, vol. 26, no. 18, pp. 1809–1812, Sep. 15, 2014.

[14] P. S. J. Russell, "Photonic-crystal fibers," *J. Lightw. Technol.*, vol. 24, no. 12, pp. 4729–4749, Dec. 2006.

[15] H. Ahmad, M. R. K. Soltanian, C. H. Pua, M. Alimadad, and S. W. Harun, "Photonic crystal fiber based dual-wavelength Q-switched fiber laser using graphene oxide as a saturable absorber," *Appl. Opt.*, vol. 53, no. 16, pp. 3581–3586, Jun. 2014.

[16] H. Ahmad, M. Soltanian, M. Alimadad, and S. Harun, "Stable narrow spacing dual-wavelength Q-switched graphene oxide embedded in a photonic crystal fiber," *Laser Phys.*, vol. 24, no. 10, Aug. 2014, Art. ID 105101.
[17] M. Soltanian, H. Ahmad, C. Pua, and S. Harun, "Tunable microwave output over a wide RF region generated by an optical dual-wavelength fiber laser," *Laser Phys.*, vol. 24, no. 10, Aug. 2014, Art. ID 105116.
[18] M. R. K. Soltanian, I. S. Amiri, S. E. Alavi, and H. Ahmad, "Dual-wavelength erbium-doped fiber laser to generate terahertz radiation using photonic crystal fiber," *J. Lightw. Technol.*, vol. 33, no. 24, pp. 5038–5046, Dec. 2015.
[19] W. Chen *et al.*, "Switchable multi-wavelength fiber ring laser based on a compact in-fiber Mach–Zehnder interferometer with photonic crystal fiber," *Laser Phys.*, vol. 19, no. 11, pp. 2115–2119, Nov. 2009.
[20] H. Ahmad, M. R. K. Soltanian, C. H. Pua, M. Z. Zulkifli, and S. W. Harun, "Narrow spacing dual-wavelength fiber laser based on polarization dependent loss control," *IEEE Photon. J.*, vol. 5, no. 6, Dec. 2013, Art. ID 1502706.
[21] M. P. Fok and C. Shu, "Tunable dual-wavelength erbium-doped fiber laser stabilized by four-wave mixing in a 35-cm highly nonlinear bismuth-oxide fiber," *Opt. Exp.*, vol. 15, no. 10, pp. 5925–30, May 14, 2007.
[22] C. Mou *et al.*, "Single- and dual-wavelength switchable erbium-doped fiber ring laser based on intracavity polarization selective tilted fiber gratings," *Appl. Opt.*, vol. 48, no. 18, pp. 3455–3459, Jun. 20, 2009.
[23] R. Parvizi, N. M. Ali, S. W. Harun, and H. Ahmad, "Architecture of a dual-wavelength Brillouin fibre laser based on a photonic crystal fibre with dual-pass amplification configuration," *Lasers in Engineering*, vol. 21. Philadelphia, PA, USA: Old City, 2011, pp. 209–216.
[24] M. Scheller *et al.*, "Room temperature continuous wave milliwatt terahertz source," *Opt. Exp.*, vol. 18, no. 9, pp. 27112–27117, Dec. 2010.
[25] A. Melloni and M. Martinelli, "Synthesis of direct-coupled-resonators bandpass filters for WDM systems," *J. Lightw. Technol.*, vol. 20, no. 2, pp. 296–303, Feb. 2002.
[26] A. Melloni, R. Costa, P. Monguzzi, and M. Martinelli, "Ring-resonator filters in silicon oxynitride technology for dense wavelength-division multiplexing systems," *Opt. Lett.*, vol. 28, no. 17, pp. 1567–1569, Sep. 2003.
[27] M. A. Popovíc *et al.*, "Multistage high-order microring-resonator add-drop filters," *Opt. Lett.*, vol. 31, no. 17, pp. 2571–2573, Sep. 2006.
[28] H. Ahmad, M. Soltanian, I. Amiri, S. Alavi, and A. Supaat, "Carriers generated by mode-locked laser to increase serviceable channels in radio over free space optical systems," *IEEE Photon. J.*, vol. 7, no. 5, Oct. 2015, Art. ID 7904112.
[29] I. Amiri *et al.*, "Experimental measurement of Fiber-Wireless (Fi-Wi) transmission via multi mode locked solitons from a ring laser EDF cavity," *IEEE Photon. J.*, vol. 7, no. 2, Apr. 2015, Art. ID 7100709.
[30] M. Soltanian, I. Amiri, S. Alavi, and H. Ahmad, "All optical ultra-wideband signal generation and transmission using mode-locked laser incorporated with add–drop microring resonator," *Laser Phys. Lett.*, vol. 12, no. 6, May 2015, Art. ID 065105.
[31] I. Amiri, M. Soltanian, S. Alavi, and H. Ahmad, "Multi wavelength mode-lock soliton generation using fiber laser loop coupled to an add–drop ring resonator," *Opt. Quantum Electron.*, vol. 47, no. 8, pp. 2455–2464, Aug. 2015.
[32] I. S. Amiri *et al.*, "W-band OFDM transmission for radio-over-fiber link using solitonic millimeter wave generated by MRR," *IEEE J. Quantum Electron.*, vol. 50, no. 8, pp. 622–628, Aug. 2014.
[33] A. Arbabi, Y. M. Kang, C.-Y. Lu, E. Chow, and L. L. Goddard, "Realization of a narrowband single wavelength microring mirror," *Appl. Phys. Lett.*, vol. 99, no. 9, Aug. 2011, Art. ID 091105.
[34] H. A. Haus, "Mode-locking of lasers," *IEEE J. Sel. Topics Quantum Electron.*, vol. 6, no. 6, pp. 1173–1185, Nov./Dec. 2000.
[35] C. Ironside *et al.*, "Review of optoelectronic oscillators based on mode locked lasers and resonant tunneling diode optoelectronics," in *Proc. Int. Conf. Appl. Opt. Photon.*, 2011, Art. ID 80011Q.
[36] L. O. Lierstuen and A. S. Sudbø, "Coupling losses between standard single-mode fibers and rectangular waveguides for integrated optics," *Appl. Opt.*, vol. 34, no. 6, pp. 1024–1028, Feb. 1995.
[37] M. A. Mentzer, *Applied Optics Fundamentals and Device Applications: Nano, MOEMS, and Biotechnology*. Boca Raton, FL, USA: CRC, 2011.
[38] M. Robertson, S. Ritchie, and P. Dayan, "Semiconductor waveguides: Analysis of coupling between rib waveguides and optical fibres," in *Proc. SPIE Integr. Opt. Circuit Eng.*, 1985, pp. 184–191.
[39] I. S. Amiri *et al.*, "Increment of access points in integrated system of wavelength division multiplexed passive optical network radio over fiber," *Sci. Rep.*, vol. 5, 2015, Art. ID 11897.